Two-photon brightness of azobenzene photoswitches designed for glutamate receptor optogenetics

Elizabeth C. Carroll[a], Shai Berlin[a], Joshua Levitz[a], Michael A. Kienzler[a], Zhe Yuan[a], Dorte Madsen[b], Delmar S. Larsen[b], and Ehud Y. Isacoff[a,c,d,1]

[a]Department of Molecular and Cell Biology, University of California, Berkeley, CA 94720; [b]Department of Chemistry, University of California, Davis, CA 95616; [c]Helen Wills Neuroscience Institute, University of California, Berkeley, CA 94720; and [d]Physical Bioscience Division, Lawrence Berkeley National Laboratory, Berkeley, CA 94720

Edited by Winfried Denk, Max Planck Institute for Medical Research, Heidelberg, Germany, and approved January 7, 2015 (received for review September 9, 2014)

Mammalian neurotransmitter-gated receptors can be conjugated to photoswitchable tethered ligands (PTLs) to enable photoactivation, or photoantagonism, while preserving normal function at neuronal synapses. "MAG" PTLs for ionotropic and metabotropic glutamate receptors (GluRs) are based on an azobenzene photoswitch that is optimally switched into the liganding state by blue or near-UV light, wavelengths that penetrate poorly into the brain. To facilitate deep-tissue photoactivation with near-infrared light, we measured the efficacy of two-photon (2P) excitation for two MAG molecules using nonlinear spectroscopy. Based on quantitative characterization, we find a recently designed second generation PTL, L-MAG0$_{460}$, to have a favorable 2P absorbance peak at 850 nm, enabling efficient 2P activation of the GluK2 kainate receptor, LiGluR. We also achieve 2P photoactivation of a metabotropic receptor, LimGluR3, with a new mGluR-specific PTL, D-MAG0$_{460}$. 2P photoswitching is efficiently achieved using digital holography to shape illumination over single somata of cultured neurons. Simultaneous Ca^{2+}-imaging reports on 2P photoswitching in multiple cells with high temporal resolution. The combination of electrophysiology or Ca^{2+} imaging with 2P activation by optical wavefront shaping should make second generation PTL-controlled receptors suitable for studies of intact neural circuits.

optogenetics | pharmacology | multiphoton | photoswitch | azobenzene

Modern neurobiology relies heavily on optical microscopy to observe, and, increasingly, to manipulate (1, 2), biological processes in live tissue. Among these methods, 2-photon-excited fluorescence microscopy (2PM) with near-infrared (NIR) light has emerged as an important technique for extending optical microscopy to highly scattering tissue (3, 4). Remarkably, barely 25 years after the first 2P-excited fluorescence image was published (5), 2PM is now performed in awake, behaving animals (4, 6–8). Naturally, optical manipulations in the brain can benefit from the many advantages of 2PM (9). In particular, the inherent spatial confinement of 2P absorption is critical for optical manipulation of individual cells (10) in the intact mammalian brain, where it is difficult to control the spatial extent of gene expression or confine soluble reagents. However, 2P-excited optogenetics is not yet as widespread in adoption as 2PM, being widely perceived to require sophisticated optical techniques (11–13) or reagent concentrations that compromise pharmacological specificity (2, 14).

The rapid time to adoption of 2PM owes at least some credit to the availability of spectroscopic data on the 2P-excited efficacy, or brightness, of synthetic and genetically encoded fluorophores (15–17). Brightness, defined for fluorophores as the product of absorption cross-section and fluorescence quantum yield, gives the experimenter an objective metric to assess fluorescent reporters and identify appropriate optical parameters, such as the optimal excitation wavelength and range of light intensities (18). By comparison, relatively little information is available on the 2P properties of optogenetic and photopharmacological tools (12, 14). Wider adoption of 2P optical manipulations should follow from quantitative characterization of 2P brightness for optogenetic and photopharmacological reagents.

Here we quantify the 2P brightness of two types of photoswitchable tethered ligands (PTLs) based on azobenzene. PTLs comprise a modular class of genetically-targeted photochemical tools first conceived in the 1970s by Eranger and Lester for acetylcholine receptors (19, 20). PTLs have since been developed for a variety of other receptors and channels (2). Maleimide-azobenzene-glutamate (MAG) compounds are designed to be conjugated to the extracellular ligand binding domains of genetically engineered mammalian glutamate receptors (GluRs), enabling pharmacological manipulation of signaling pathways dependent on the excitatory neurotransmitter glutamate (21–25). MAGs have been used to study neurotransmission and neuroplasticity in a variety of preparations (26–29). Two families of MAGs have been synthesized to date: First generation MAGs have a symmetrically-substituted azobenzene core, e.g., L-MAG0 (21) and D-MAG0 (30). Second generation MAGs have an asymmetrically-substituted azobenzene core, e.g., L-MAG0$_{460}$ (31) and MAG$_{2p}$ (32). The latter MAGs are single-color photoswitches incorporating an electron-donating amine and an electron-withdrawing amide substitution, creating a "push–pull" system that both red-shifts the *trans* isomer absorption spectrum and reduces the thermal stability of the *cis* isomer (31, 33).

Significance

MAGs (maleimide-azobenzene-glutamate) are photoswitches that covalently bind to genetically engineered glutamate receptors (GluRs) and, under the control of light, mimic or block the action of the excitatory neurotransmitter glutamate. However the blue and near-UV light that optimally photoswitch MAGs do not penetrate well into the brain. In this paper, we show how MAGs can instead be photoswitched by two-photon (2P) absorption of near-infrared light, which penetrates deeper into tissue. We demonstrate 2P control of MAG-dependent ionic currents in neurons, and synthesize a new MAG photoswitch to enable 2P activation of a G protein coupled receptor signaling cascade through a metabotropic GluR. These optogenetic tools bring exceptional spatiotemporal resolution and pharmacological specificity to the study of synaptic transmission and plasticity in intact neural circuits.

Author contributions: E.C.C., S.B., J.L., M.A.K., D.S.L., and E.Y.I. designed research; E.C.C., S.B., J.L., M.A.K., and D.M. performed research; M.A.K. and Z.Y. contributed new reagents/analytic tools; E.C.C., M.A.K., and D.M. analyzed data; and E.C.C., S.B., M.A.K., D.S.L., and E.Y.I. wrote the paper.

The authors declare no conflict of interest.

This article is a PNAS Direct Submission.

[1]To whom correspondence should be addressed. Email: ehud@berkeley.edu.

This article contains supporting information online at www.pnas.org/lookup/suppl/doi:10.1073/pnas.1416942112/-/DCSupplemental.

It was recently reported that the asymmetric substitution in second generation PTLs enabled efficient 2P excitation in two antennae-bearing PTLs, MAG_{2p}, and $MAGA_{2p}$ (32). However, that study concluded that the bistable nature of a first generation MAG could ultimately generate a larger effect, albeit at a slower rate, by building up a population of *cis* isomers. We spectroscopically characterized L-MAG0 and the original "push–pull" MAG, L-$MAG0_{460}$, in solution, and determined the 1P and 2P absorption cross-sections and quantum yield of photoisomerization for these molecules. From experimental values, we determine that 2P-excited *trans* → *cis* photoswitching in L-$MAG0_{460}$ occurs with efficiency comparable to 2P-excited fluorescence in EGFP (18). In other words, L-$MAG0_{460}$ is as bright as EGFP. However, owing to a symmetry-disallowed 2P transition to the near-UV absorption band, L-MAG0 and other first generation PTLs are ill-suited to the range of wavelengths most commonly used for 2PM (700–1,100 nm).

We validate these spectroscopic results with functional characterization of 2P photoactivation of MAGs in cultured cells expressing genetically engineered glutamate receptors, identifying sets of parameters suitable for 2P photoactivation of MAGs in several GluR–PTL combinations: We demonstrate that 2P excitation with 800–900-nm pulses efficiently activates LiGluR photocurrents in neurons labeled with L-$MAG0_{460}$, but not with L-MAG0. Using digital holography (2P-DH) (13, 34), we demonstrate that activation of L-$MAG0_{460}$ is compatible with functional imaging using the red genetically encoded calcium indicator R-GECO1.0 (35). This combination of optical tools facilitates fast, multicellular stimulation and recording, an important benchmark for the utility of PTLs for in vivo optogenetic studies. Finally, we synthesized a new compound with altered stereochemistry, and show that the resulting PTL, D-$MAG0_{460}$, enables 2P control of an engineered G protein-coupled receptor (GPCR), LimGluR3 (30). We discuss why the 2P optical properties of MAGs generalize to a larger range of ligand substitutions, which could broaden the palette of PTLs for optogenetic neural circuit analysis in tissue.

Results

One-Photon Absorption. The 1P absorption spectra of the first and second generation MAGs, L-MAG0 and L-$MAG0_{460}$, in DMSO are shown in Fig. 1 (blue solid lines). The absorption spectra of these PTLs can be described by inhomogenously broadened bands (Fig. 1, dashed lines) similar in relative strength and energies to the two lowest energy optical transitions in the core azobenzenes: *Trans*-L-MAG0 (Fig. 1*A*) has a near-UV absorption peak at 376 nm, with a much weaker transition at 450 nm, consistent with π-π* and n-π* electronic transitions in the substituted core, bis-*para*-diamidoazobenzene (36). The strength of these bands is altered in *cis*-L-MAG0 (Fig. 1*B*), which is sufficiently metastable that it can be measured with a conventional spectrophotometer by first generating a photostationary state with near-UV light. Second generation *trans*-L-$MAG0_{460}$ has two overlapping visible absorption bands (Fig. 1*C*, dashed lines), which can be resolved by looking at the solvent dependence of the 1P absorption spectrum (*SI Appendix*, Fig. S1). As in the parent compound Disperse Red 1, these data support assignment of n-π* and π-π* electronic transitions (37, 38). We determined an extinction coefficient, $\varepsilon = 19{,}500 \pm 500\ M^{-1}\ cm^{-1}$ at 425 nm in DMSO. The spectrum of *cis*-L-$MAG0_{460}$ was determined by transient absorption (see below).

Two-Photon Absorption. MAGs are not fluorescent, so we measured the 2P absorption cross-section spectra (σ_2 spectra) directly using a nondegenerate white light continuum technique (39) (described in detail in *SI Appendix*, Figs. S2 and S3). The resulting spectra revealed strikingly different 1P and 2P absorption properties in the *trans* isomers of both MAGs (Fig. 1 *A* and *C*, red symbols). The peak absorption ($\lambda_{eff} = 318 \pm 2$ nm) in first generation compound *trans*-L-MAG0 was blue-shifted 4,850 cm^{-1} relative to the 1P absorption peak ($\lambda = 376$ nm in DMSO) (Fig. 1*A*), which is more consistent with a higher energy transition that does not appear in the 1P spectrum. When the 2P measurement was repeated in the background of a photostationary population of *cis* isomers, the 318-nm absorption markedly, and reversibly, decreased in intensity while absorption at the n-π* transition increased (Fig. 1*B*, red symbols). Based on additional 2P measurements on a related PTL (maleimide-azobenzene-quaternary ammonium) in phosphate buffered solution (*SI Appendix*, Fig. S4), we saw no evidence that peak at 318-nm peak was grossly influenced either by solvent polarity or by resonance-enhanced 2P absorption due to overlap between the white light and 1P absorption spectra (*SI Appendix*). *Trans*-L-$MAG0_{460}$ had peak σ_2 at the same transition energy as peak 1P absorption ($\lambda_{eff} = 427$ nm), but dropped off more steeply at low energies, resolving the n-π* absorption band (Fig. 1*C*, red

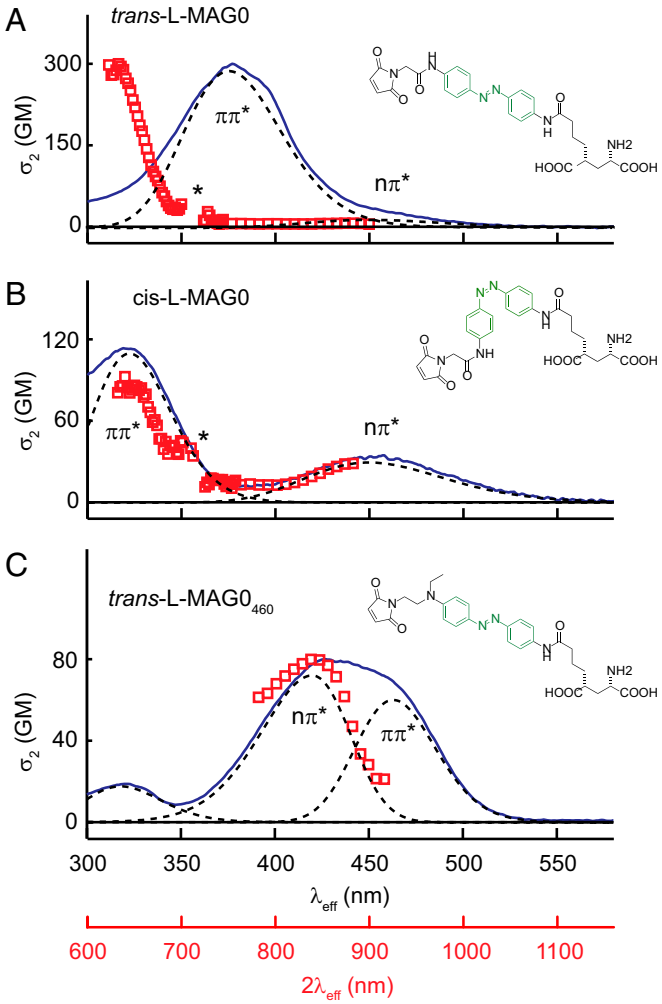

Fig. 1. Two photon absorption spectra of MAGs. Experimental 1P (blue solid line) and 2P absorption spectra (red open squares) for azobenzenes-derived MAGs (*A*) *trans*-L-MAG0, (*B*) *cis*-L-MAG0, (*C*) *trans*-L-$MAG0_{460}$ in DMSO. The λ_{eff} and $2\lambda_{eff}$ axes represent the transition energy as the wavelength required for 1P or degenerate 2P absorption, respectively. The azobenzene core is highlighted in green. Spectra were decomposed into bands representing inhomogenously broadened electronic transitions (dashed lines) from σ- or π-character valence electron molecular orbitals to an antibonding excited state (π*). In *A* and *B*, an asterisk indicates regions where measure of σ_2 was unreliable due to Raman scattering of λ_{NIR} (*SI Appendix*).

symbols). Taken together, the 2P absorption spectra of both MAGs are consistent with parity selection rules for dipolar transitions in centrosymmetric molecules. These rules predict that the lowest-energy 1P-allowed π-π* transition should be strictly forbidden for 2P absorption (9).

Molecular 2P absorption cross-sections (σ_2) in Goeppert-Mayer units (Table 1; 1 GM = 10^{-50} cm$^4 \cdot$ s $\cdot \gamma^{-1}$) were determined from back-to-back measurements of MAGs and reference samples (*SI Appendix*, Figs. S3*I* and S5*E*). The resulting σ_2 values (Table 1) are remarkably consistent with those of the parent compounds and related compounds from both classes of azobenzenes (36, 38). Notably, the σ_2 of both MAGs are orders of magnitude larger than that of the most widely used caged neurotransmitter, MNI-glutamate ($\sigma_2 = 0.04 \pm 0.02$ GM at 730 nm; ref. 40). The cross-section of *trans*-L-MAG0$_{460}$ is at least as large as the most common fluorescent proteins (σ_2 = 40–100 GM; ref. 17) in the NIR.

Quantum Yield of MAG Photoisomerization. Brightness depends not only on the strength of absorption, but also on the quantum efficiency of the process of interest. To ascertain the quantum yield (QY) of *trans* → *cis* photoisomerization (denoted E→Z), we characterized the excited state reaction of the isolated MAGs in solution using broadband femtosecond transient absorption spectroscopy (*SI Appendix*, Fig. S2). Following excitation with 400-nm 100-fs laser pulses, time-resolved difference spectra were obtained with 150-fs resolution for the first 1 ns of the reaction (Fig. 2). In both MAGs, the kinetics near the peak 1P absorption show an instrument-limited transient bleach of the *trans* isomer (Fig. 2*A*, λ_{probe} = 380 nm; Fig. 2*C*, λ_{probe} = 420 nm) that partially recovers as a fraction of photoexcited molecules isomerize. The bleach decay occurs on two distinct timescales, mirrored in the kinetics of a red-shifted absorption (Fig. 2*B*, λ_{probe} = 460 nm; Fig. 2*D*, λ_{probe} = 540 nm). These time- and wavelength-resolved datasets were decomposed by global analysis (41) using a multistate model based on the photodynamics of *trans*-azobenzene (42) (*SI Appendix*, Fig. S6). In L-MAG0, we found a net photoproduct yield, $\varphi^{E\rightarrow Z} = 0.15 \pm 0.05$, which is within the range of reported values for *trans–cis* photoisomerization in azobenzene in DMSO via π-π* excitation (43). The difference spectrum associated with the photoproduct (Fig. 2*B*, *Upper*, green solid line) nicely decomposed into the *cis* and *trans* spectra derived from photostationary measurements (Fig. 2*B*, *Lower*, green circles). Furthermore, from knowledge of the extinction coefficients of both isomers and the yield of the forward reaction, we can infer from photostationary spectra that the QY of cis-trans isomerization is 0.4, consistent with cis-azobenzene (42).

The L-MAG0$_{460}$ data were fit to the same model to obtain $\varphi^{E\rightarrow Z} = 0.4 \pm 0.1$. A higher isomerization QY is consistent with excitation of the n-π* transition (42). The photoproduct spectrum had a red-shifted band (Fig. 2*D*, *Lower*, green circles), qualitatively consistent with a *cis* isomer (42). However, the 1-ns absorption spectrum extends to longer wavelengths than observed in photostationary measurements on related compounds (32), and may represent a vibrationally "hot" *cis*-L-MAG0$_{460}$. Transient absorption following 2P excitation with the laser fundamental (800 nm, 100 fs, 16 mW) produced a similar photoproduct (Fig. 2*D*, *Lower*, red solid line). Thus, it appeared that 1P and 2P excitation in *trans*-L-MAG0$_{460}$ are both effective at driving *trans–cis* photoisomerization.

From the experimental values for ε, σ_2, and φ, the brightness of each MAG isomer was defined as εφ and $\sigma_2\varphi$, for 1P and 2P excitation, respectively (Table 1). The *trans* isomer brightness represents the probability of photoswitching from the thermally equilibrated (dark) state. Compared with the 2P brightness of common fluorescent reports like EGFP (30 GM at 927 nm; ref. 17), these brightness values indicate that *trans*-L-MAG0$_{460}$ is favorably suited for the NIR light sources and intensities typical in 2PM. *Trans*-L-MAG0, on the other hand, is at least 20 times dimmer at NIR wavelengths. Whereas the large cross-section at 640 nm suggests that L-MAG0 might be a powerful tool if used in conjunction with visible-wavelength femtosecond light sources, the QY of this 1P-disallowed remains to be determined to properly quantify brightness.

Two-Photon *Cis–Trans* Photoswitching of L-MAG0. We next sought to validate 2P excitation of MAGs through functional measurements in live cells expressing engineered GluRs. For GluRs engineered to be agonized by the *cis* isomer, bistable L-MAG0 can mimic the chronic effect of soluble GluR agonists, with the unique feature of very fast and reversible action (23). The strength of MAG agonism is intrinsically limited by the largest population of *cis* isomers that can be attained, which is defined by the wavelength-dependent photostationary state (PSS). Based on the σ_2 spectra (Fig. 1), different PSS can be expected under 1P and 2P excitation. In fact, the *cis* isomer is significantly brighter than the *trans* isomer for wavelengths greater than 700 nm. Consequently, starting from a dark-equilibrated population of *trans* isomers, the rate of *trans* → *cis* 2P activation would quickly be exceeded by the rate of *cis* → *trans* 2P de-activation, tending to "turn off" the MAG effect. Therefore, we expected that L-MAG0 would inherently produce weaker *cis*-agonism under 2P excitation than under 1P excitation.

To test these predictions, we measured L-MAG0-activated photocurrents in the engineered GluK2 kainate receptor, LiGluR, using whole cell patch clamping on a laser-scanning microscope equipped with 405 nm and 488 nm lasers, as well as a Ti:sapphire laser (Fig. 3). Dissociated hippocampal neurons were transfected with an hSyn (human synapsin 1) gene promoter driven LiGluR (GluK2-L439C-K456A), where L439C is known to bind L-MAG0 as a *cis*-activated agonist (21–24) (Fig. 3*A*). The additional point mutation (K456A) reduces affinity for soluble glutamate and quickens receptor recovery to glutamate-dependent desensitization (44, 45). Photocurrents were induced by scanning the imaging laser over the patched cell somata and proximal processes (Fig. 3*B*, red dashed lines). The 1P excitation

Table 1. Brightness of glutamate photopharmaceuticals

Compound	ε (M^{-1} cm^{-1}) [λ_{max}]	φ	εφ	σ_2 (GM) [λ_{max}]	$\sigma_2\varphi$
trans L-MAG0$_{460}$	19,500 [425]	0.4	8,000	80 [850]	32
trans L-MAG0	28,000 [376]	0.15	4,200	300 [630]	n.d.
				10 [820]	1.5
cis-L-MAG0	2,000† [450]	0.4‡	800	95 [640]	n.d.
				32 [900]	12
MNI-glutamate*	4,300 [330]	0.085	365	0.04 [730]	0.003
RuBi-glutamate*	5,600 [450]	0.13	728	n.d.	n.d.

n.d. = not determined.
*Ref. 14.
†Ref. 60.
‡Inferred from PSS of 96% *cis* isomers at 380 nm (22).

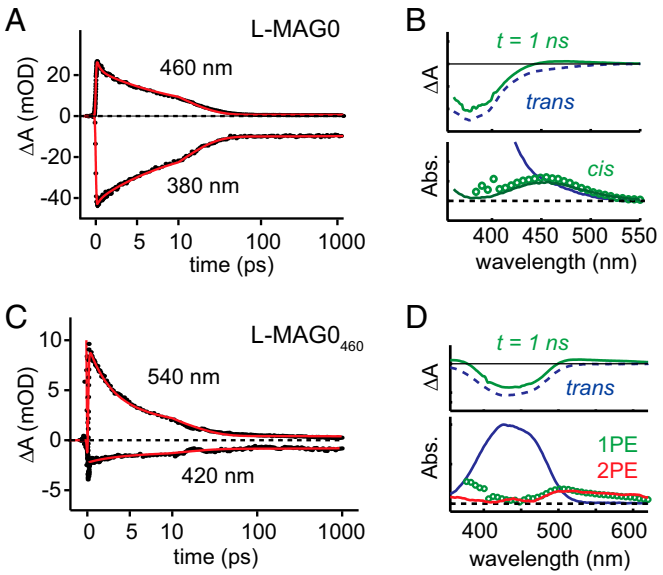

Fig. 2. Photoisomerization dynamics in MAGs. (*A*) Time-resolved changes in absorption for select wavelengths during *trans–cis* photoisomerization reaction in L-MAG0. The time axis is linear until 10 ps, and logarithmic thereafter. Kinetics at λ_{probe} = 380 nm, near the peak 1P absorption of *trans*-L-MAG0, show the transient bleach and recovery of photoexcited molecules that do not undergo isomerization. Kinetics at λ_{probe} = 460 nm represent vibrationally excited isomerization photoproducts. Solid red lines represent fits obtained from global analysis (*SI Appendix*, Fig. S6). (*B*) The 1-ns difference spectrum (*Upper*, green solid line) was decomposed into *trans* (*Upper*, blue dashed; *Lower*, blue solid) and *cis* contributions. The putative *cis* spectrum (*Lower*, green circles) closely matches that of *cis*-L-MAG0, derived from photostationary measurements (*Lower*, green solid line). (*C*) Kinetics in the photoisomerization of *trans*-L-MAG0$_{460}$ were similar, with *trans* isomer dynamics represented by the kinetics at λ_{probe} = 420 nm, and photoproduct dynamics seen at λ_{probe} = 540 nm. Solid red lines represent fits obtained from global analysis. (*D*) The 1-ns difference spectrum (*Upper*, green solid) was decomposed into *trans* (*Upper*, black dashed; *Lower*, solid blue) and a putative *cis* (green circles) absorption spectra with isomerization QY of 0.4 ± 0.1. The 2P excitation yielded a similar photoproduct (*Lower*, red solid).

with 405 nm generated a saturated photocurrent that was reversible with 488 nm (Fig. 3*C*, *i*, purple and green bars, respectively), consistent with previous studies on LiGluR (23). Scanning over the same region with a Ti:sapphire imaging laser (80-MHz repetition rate, time-averaged intensity < 20 mW/μm^2) with wavelengths in the range 800–900 nm produced reversible inward currents with much slower onset (Fig. 3*C*, *ii*, yellow bars). The 2P photocurrents elicited in this manner never exceeded 15% of 1P photocurrents from the same cell (Fig. 3*D*, n = 8 with at least one 2P wavelength tested per cell), despite scan periods as long as 10 s. This value is consistent with the 2P PSS expected at 900 nm from the relative 2P brightness of *trans* and *cis* isomers of L-MAG0 (Table 1).

Next, we tested 2P deactivation of LiGluR photocurrents. Again, a 405-nm laser was scanned over the soma to generate a saturated photocurrent, where ∼90% of the MAG molecules are in *cis* conformation. When the 2P laser was subsequently scanned over the same area, we observed a reversible reduction in photocurrent indicative of *cis* → *trans* photoswitching (Fig. 3C, *iii*, yellow, red, and brown bars and summary in Fig. 3*E*). The rate of photocurrent reduction was consistent with the measured σ_2 spectrum of the *cis* isomer (Fig. 1*B*), although we found that often photocurrents continued to decrease even after 2P exposure ceased, suggesting that prolonged NIR exposure might additionally affect thermal reisomerization. Together, these results demonstrate that, although it is possible to weakly activate LiGluR + L-MAG0 by 2P excitation, 2P deactivation is the more efficient process, which intrinsically limits the efficacy of L-MAG0 when used at Ti:sapphire laser wavelengths.

Fast 2P Photoswitching of L-MAG0$_{460}$ in Cultured Neurons with 2P Digital Holography. Many optogenetic applications require manipulating select cells within a population with high spatiotemporal precision. Two-photon digital holography (2P-DH) is an effective method to flexibly target light to many regions simultaneously, or to produce an extended image to excite large patches of membrane for summation of single-channel ionic currents (13). It was recently shown that 2P scanning excitation of MAG$_{2p}$ could depolarize neurons, but scans of nearly 1 s were necessary (32). We asked whether faster photoactivation might be attained with 2P-DH.

To test activation of *trans*-L-MAG0$_{460}$ by 2P-DH, we again transfected dissociated hippocampal neurons with LiGluR. It was shown previously that L-MAG0$_{460}$ covalently tethered to position L439C activates the channel under blue light, while photocurrent decreases in the dark by thermal isomerization of L-MAG0$_{460}$ (22). Here, 1P stimulation was achieved with a 470-nm LED used as a wide-field light source that illuminated the entire neuron (Fig. 4*A*, image, blue shadow). The 50–100-ms pulses of blue light elicited LiGluR photocurrents of a stereotypical shape (Fig. 4*A*, traces): Photocurrent switched on rapidly, reached a peak current (S_{max}) that was approximately sustained through the duration of the stimulation pulse and decayed slowly (relative to onset) following the end of the light pulse. S_{max} varied between cells (30–400 pA, mean = 80 ± 20 pA, n = 20). In many neurons, 1P excitation triggered action potentials in unclamped portions of the cell (seen as action currents, indicated by * in Fig. 4*A*).

For 2P excitation, light was targeted to the soma of each neuron (Fig. 4*B*, image, red region) by spatially patterning laser pulses from a Ti:sapphire laser using digital holography (13). Bouts of 50–100 ms of 840–850-nm robustly generated photocurrents (Fig. 4*B*, traces) that were similar to those evoked by 1P excitation. The decays of 1P and 2P photocurrents were nearly identical (Fig. 4 *C* and *D*: $\tau_{1/2}$ = 200 ± 10 ms for 1P, n = 20; $\tau_{1/2}$ = 190 ± 20 ms for 2P, n = 11; p = 0.3, unpaired, two-way t test). These photocurrent kinetics are slightly faster than previous observations in HEK293 cells of 1P activation of GluK2-L439C where glutamate desensitization was blocked with concavalin A (31), suggesting that both thermal isomerization of L-MAG0$_{460}$ and LiGluR channel dynamics contribute to photocurrent decay. Regardless, the effective decay kinetics do not depend on 1P vs. 2P excitation, nor on somatic vs. whole cell excitation, supporting our interpretation that the photocurrents arise from the same photopharmacological process.

The 2P-DH excitation with time-averaged intensity in the range of 1–2.3 mW/μm^2 stimulated photocurrents that were 38 ± 8% of the maximum current reached by 1P excitation of the same neuron (Fig. 4*E*, n = 11). The generation of smaller photocurrents by 2P-DH was consistent with the smaller fraction of the cell that was illuminated (compare blue region to red region in Fig. 4 *A* and *B*, respectively) considering that studies showed that LiGluR overexpressed in neurons is distributed throughout the plasma membrane (23, 46). Additional analysis of photoswitching efficiency is presented in *SI Appendix* (*SI Appendix*, Fig. S7).

Simultaneous Ca^{2+}-Imaging and 2P-DH Photoswitching. Another major challenge in optogenetics is how to stimulate and measure physiological function without interference between optical reporters and effectors. Thus, we next asked whether 2P-DH photoswitching of L-MAG0$_{460}$ would be compatible with simultaneous functional imaging. Because LiGluR is Ca^{2+}-permeable, we measured photoactivation of LiGluR + L-MAG0$_{460}$ with the genetically encoded red fluorescent Ca^{2+} indicator, R-GECO1.0

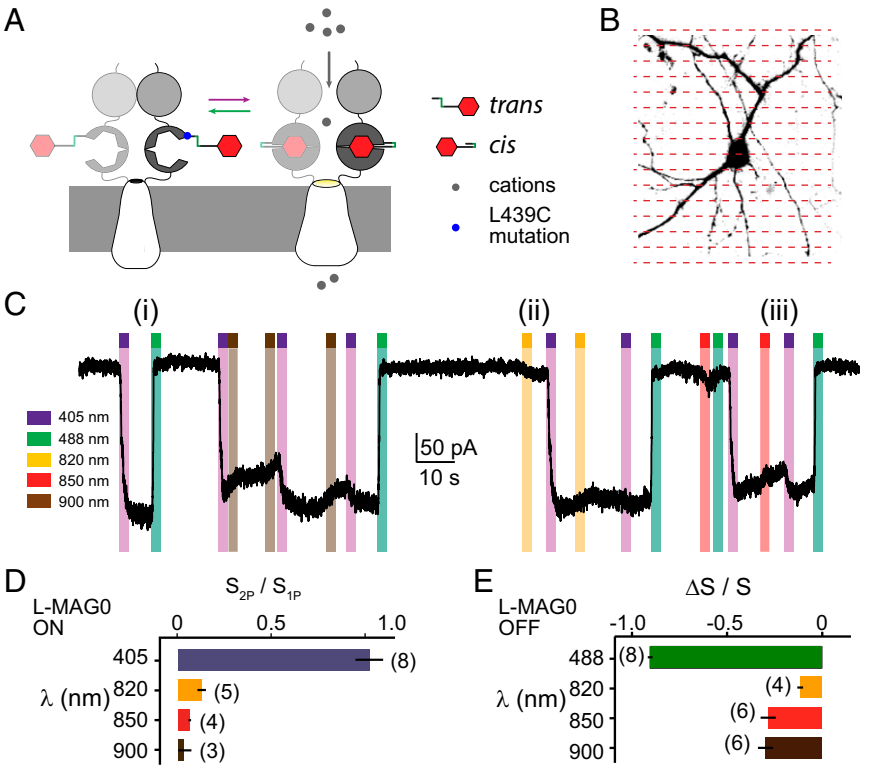

Fig. 3. *Cis-trans* 2P photoswitching is favored for L-MAG0. (*A*) The 2P photoswitching of L-MAG0 was assessed by LiGluR photocurrents. *Trans–cis* isomerization of MAG docks the glutamate moiety in the ligand binding domain, causing the channel to open and pass an inward ionic current. (*B*) Cultured neurons expressing LiGluR and labeled with L-MAG0 were patch clamped and photoactivated on a laser-scanning microscope. (*C*) Representative whole cell voltage-clamp recording showing the effects of 1P and 2P laser-scanning excitation. Each colored bar represents a stimulation period during which laser light at the designated wavelength was rastered bidirectionally over the cell somata: (*i*) 405-nm light reproducibly elicited saturated, bistable photocurrents reversible with 488 nm. (*ii, iii*) Starting from a 1P-saturated LiGluR photocurrent, 2P stimulation reversibly decreased the amplitude of photocurrent, indicating closure of LiGluR channels by *cis–trans* photoswitching. (*D*) At the highest intensities tolerated by the cells (20 mW/μm^2 time-averaged intensity), 2P laser scanning generated photocurrents no greater than 15% of the photocurrents stimulated by 405-nm laser scanning of the same cell. Bars were calculated as the mean current photoactivated from a dark resting state for 2–6 photoswitching cycles, normalized to the cell's 1P response, and then averaged across cells. The number of independent cells measured at each wavelength is denoted in parentheses. Error bars are SEM. (*E*) Bars represent the mean relative change in current from two to four photoswitching cycles, averaged across cells. Error bars are SEM.

(35) (Fig. 5). Previous work demonstrated that 1P activation of L-MAG0$_{460}$ at 560 nm does not generate significant LiGluR photocurrent (31); consequently, we reasoned that imaging R-GECO1.0 at this wavelength would produce little background MAG activation. Initial tests in HeLa cells expressing LiGluR showed that following whole-cell 2P-DH stimulation with 840 nm (100 ms exposure at 0.3–1.1 mW/μm^2), R-GECO reports Ca^{2+} transients that depend on L-MAG0$_{460}$ (Fig. 5*A*, *Upper*, red trace). In cells not treated with L-MAG0$_{460}$, 2P-DH stimulation resulted in modest bleaching of R-GECO1.0 basal fluorescence (Fig. 5*A*, *Lower*, gray trace represent fluorescence recovery after photobleaching. Because 2P bleaching of R-GECO1.0 should be independent of the PTL, L-MAG0$_{460}$-dependent rises in R-GECO1.0 fluorescence (Fig. 5*B*) likely underrepresent the actual size of the Ca^{2+} transient. Nonetheless, 2P photoswitching of L-MAG0$_{460}$ appears compatible with imaging with a red genetically encoded Ca^{2+} indicator with a reasonable signal-to-noise ratio.

To further explore the potential of all-optical, ligand-specific optogenetics, we used the combination of 2P-DH photoswitching and functional imaging to report on Ca^{2+} activity in a population of cells in response to sequential targeted 2P photostimulation. Holograms for three regions of interest (ROIs) were calculated prior to time-lapse acquisition (Fig. 5 *C* and *D*). During image acquisition, holograms were projected in sequence (1–3) with 50-ms delay between ROIs (Fig. 5*E*). We found that the three stimulated cells all yielded Ca^{2+} activity with a robust signal-to-noise ratio over repeated stimulation cycles (Fig. 5*E*, *Right*).

Two-Photon Photoactivation of an Engineered mGluR with D-MAG0$_{460}$. Finally, we sought to extend 2P MAG activation to optically manipulate intracellular signaling cascades using a photoactivatable G protein-coupled receptor (GPCR). We turned to the recently described LimGluR2 and LimGluR3, which are based on the group II mGluRs, mGluR2 and mGluR3 (30). LimGluRs allow for photoactivation of the $G_{i/o}$ signaling cascade (Fig. 6*A*) using the first generation PTL, D-MAG0, a variant of L-MAG0 with altered stereochemistry but similar optical properties. To achieve 2P stimulation, we synthesized a new red-shifted compound, D-MAG0$_{460}$ (Fig. 6*B*, *SI Appendix*). Following labeling with D-MAG0$_{460}$, activation of LimGluR2 (mGluR2-L300C) or LimGluR3 (mGluR3-Q306C) was assessed in HEK293T cells using the G protein activated inward rectifying potassium channel, GIRK, as a readout of activation of the $G_{i/o}$ signaling pathway (47). LimGluR3 showed robust photoactivation in response to blue light, while LimGluR2 was poorly activated by D-MAG0$_{460}$ (Fig. 6*C*). LimGluR3 + D-MAG0$_{460}$-dependent GIRK currents reversed in the dark on the time scale of 5–10 s (Fig. 6*D*), reflecting the slow off-kinetics of the G protein signaling cascade rather than the fast (subsecond) thermal isomerization kinetics of the PTL. In contrast to LiGluR + L-MAG0$_{460}$ (Fig. 4), the current rise time did not depend on 1P intensity and 5–8-s blue light exposure

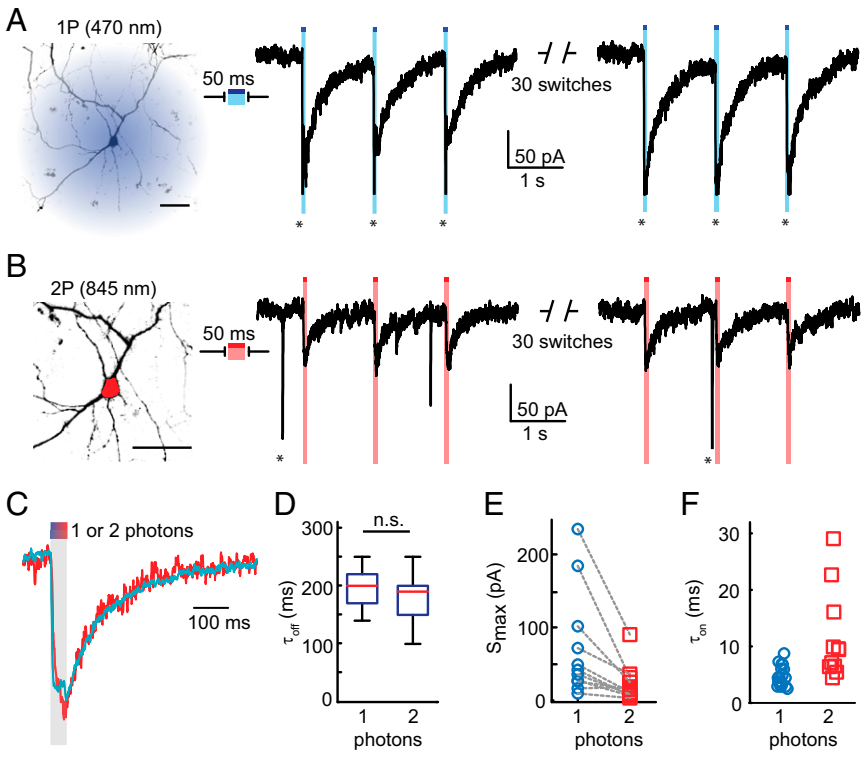

Fig. 4. LiGluR photocurrents stimulated by 1P and 2P excitation of L-MAG0$_{460}$ in cultured neurons. (*A*, *B*) Whole cell voltage-clamp recordings from the same cell following either (*A*) 1P excitation with a blue LED, or (*B*) 2P excitation targeted to the cell soma using digital holography (red ROI). The 50-ms exposure of either light source elicited long-lived ionic currents. Action currents are indicated by *. Scale bar is 20 μm. (*C*, *D*) The 1P and 2P photocurrents decayed thermally with the same rate, $\tau_{1/2}$ = 200 ± 10 ms for 1P, n = 20; $\tau_{1/2}$ = 190 ± 20 ms for 2P, n = 11; p = 0.3, 2-sample t test. All errors are SEM. (*E*) Peak photocurrents S_{max} excited by 2P-DH were 38 ± 8% of 1P photocurrents from the same cell (n = 11). (*F*) Across cells, 470 nm at 0.36 μW/μm^2 yielded an average photocurrent rise time, τ_{on} = 4.6 ± 0.4 ms (blue circles, n = 20), and 2P-DH with 845 nm at 1–2.3 mW/μm^2 yielded an average τ_{on} = 11.5 ± 2.4 ms (red squares, n = 11).

was necessary to reach a saturated signal (*SI Appendix*, Fig. S8). Because the same light intensities produced a photostationary state in L-MAG0$_{460}$, as read out by LiGluR, the slower signals suggest that photoswitching was not the rate-limiting factor in activating the G protein signaling cascade.

We next used 2P-DH to activate LimGluR3 + D-MAG0$_{460}$. Photocurrents evoked in this way by 850-nm excitation had kinetics similar to those evoked by 1P photoactivation (Fig. 6*D*). The wavelength dependence of LimGluR3 + D-MAG0$_{460}$ currents was measured by testing multiple excitation wavelengths within individual cells (Fig. 6*F*, n > 3 cells for all wavelengths). A peak at 850–860 nm is apparent, but longer wavelength produced larger signals than we expected from the L-MAG0$_{460}$ absorption spectrum (Fig. 1*A*). Upon further investigation, we observed that, in the absence of D-MAG0$_{460}$, 2P-DH illumination of cultured cells occasionally evoked inward currents that were distinguishable from LimGluR3 photocurrents by their relatively small amplitude and rapid kinetics (Fig. 6*G*, *Left*). The wavelength dependence of MAG-independent photocurrents showed that the nonspecific current increased in amplitude with longer wavelength (Fig. 6*G*, *Right*). By comparing these signals with the NIR absorption of water (48) (Fig. 6*G*, *Right*, dashed line), we conjecture that these nonspecific currents arise from heat, as has been described before in cells exposed to intense NIR laser pulses (49–51). By comparing the relative currents, normalized in each cell to the 950-nm signal, we see that the largest MAG-dependent currents occur at a wavelength of 850 nm, functionally corroborating the measured 2P absorption spectrum of L-MAG0$_{460}$ (Fig. 1*C*). Post hoc, we estimated the amplitude of MAG-dependent currents by scaling the amplitude of photocurrents by the dark relaxation kinetics, and found 2P-DH at 850 nm produced on average 85 ± 13% of the currents generated by 1P photoactivation in the same cell (Fig. 6*E*, red open squares). Because the entire cell was illuminated for both 1P and 2P excitation, the similar size of evoked currents supports comparable efficacy for 1P and 2P photoswitching of D-MAG0$_{460}$. Overall, these experiments show that D-MAG0$_{460}$ may be used to evoke mGluR3-dependent G protein signaling by 2P photoswitching, thus expanding the applications of these tools to contexts where spatial precision and deep tissue penetration are required to activate a GPCR.

Discussion

Comparison of MAGs with Other Optogenetic Tools. Because MAGs can be used for controlling neuron depolarization when tethered to an engineered ion channel (e.g., LiGluR), we note that the 2P absorption cross-sections are smaller than that of Channelrhodopsin2 (230–260 GM) (12, 39). Although it can be difficult to compare σ_2 values measured by different methods (16, 17), Yamaguchi and Tahara reported a comparable σ_2 of 230 GM for all-*trans* retinal in solution determined by the same 2P spectrophotometry technique used here (39). Because most opsins have very high QY (>0.5) for retinal isomerization, it is reasonable to expect that ChR2 is brighter than either MAG. However, L-MAG0$_{460}$ offer some flexibility in 2P excitation compared with opsins because of their relatively slow off-kinetics (52, 53). Two-photon stimulation of opsins with fast off-kinetics has required creative use of scanning algorithms (12) or scanless imaging methods (54) to achieve sufficient summation. Opsins that are specifically engineered to have slower off-kinetics can be excited by 2P laser scanning (11), although larger currents still are obtained by 2P-DH (34). Similarly, the slower thermal decay of L-MAG0$_{460}$ suggests that this PTL should be

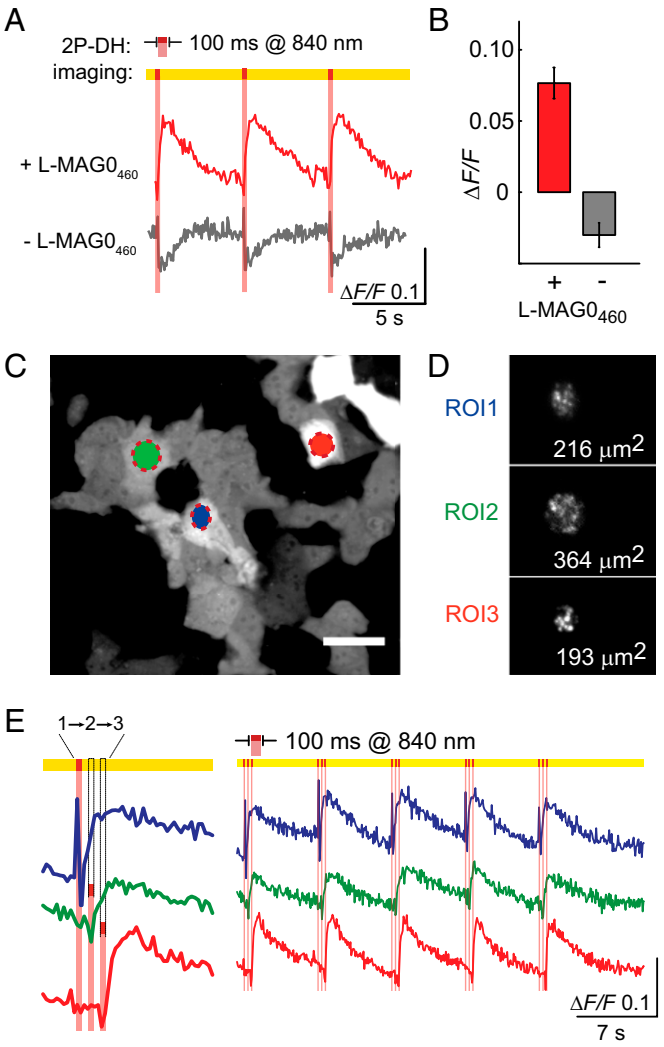

Fig. 5. The 2P-DH photoswitching of L-MAG0$_{460}$ is compatible with red Ca^{2+} imaging on a spinning disk confocal microscope. (*A*) Representative fluorescence traces from 2P-DH targeted HeLa cells coexpressing LiGluR and R-GECO1.0. (*B*) Cells not treated with MAG are bleached by 840-nm pulses (n = 6), and cells treated with L-MAG0$_{460}$ have stereotypical Ca^{2+} transients (n = 4). (*C*) Representative image of basal fluorescence of R-GECO1.0. Optical recordings were made from many cells with 50–100-ms time resolution, and 2P-DH stimulation of individual cells was targeted by encoding ROIs as separate holograms. Scale bar is 50 μm. (*D*) The fidelity of each hologram was visualized by imaging 2P-excited fluorescence from a fluorescein film. Speckles in the 2P image are common in 2P-DH. (*E*) Ca^{2+} transients recorded from three cells stimulated in rapid sequence by 840-nm projections of the holograms corresponding to *D*.

relatively insensitive to the method of 2P stimulation. Indeed, our findings of efficient 2P photoswitching of L-MAG0$_{460}$ by 2P-DH complement the recent report of two antenna-bearing MAGs with similar thermal relaxation, where LiGluR photocurrents were evoked by 2P laser scanning (32). Notably, in contrast to the study in ref. 32, our characterization in neurons was done without glutamate receptor desensitization blockers, so these optical conditions should be relevant to in vivo preparations.

Considering their ligand-specific nature, it is worthwhile to compare MAGs to other photopharmacological reagents that act on glutamate receptors. In Table 1, we compare the brightness of L-MAG0 and L-MAG0$_{460}$ with two popular types of caged glutamate (14). MNI-glutamate is still the most widely used compound in 2P applications, despite low brightness, due to its high specificity at high concentrations (2). Several other caged glutamate compounds have been developed with higher QY of photolytic cleavage or more favorable absorption at visible wavelengths (36, 37), but the 2P efficacy of most of these compounds have not been objectively quantified. Caging groups with good nonlinear absorption, such as the diethylaminocoumarin chromophore recently described by Olson et al. (55), may significantly improve the 2P efficacy of such compounds.

In general, a lack of quantitative data about these compounds limits the ability to compare optogenetic and optopharmacological tools. Characterization of 2P properties should not only help researchers select the most appropriate reagents, but also devise the most effective optical stimulation protocols. For instance, by characterizing the brightness of both isomers of L-MAG0, we showed that the maximum current one can expect from LiGluR + L-MAG0 is limited by the 2P PSS. Continued 2P exposure will not generate a larger LiGluR-specific photocurrent, and may even result in nonspecific effects as we observed in Fig. 6. On the other hand, the reasonably high 2P brightness of the *cis* isomer provides an advantage for 2P control of *trans*-activated MAGs and related azobenzene PTLs (2, 20, 25).

Two-Photon Optical Transitions in PTLs. The absorption spectra in Fig. 1 compel some consideration of parity selection rules for optical absorption. Although the early theory of Goeppert-Mayer detailed the formal extension of quantum selection rules to multiphoton transitions, these predictions could not be experimentally validated until the development of the laser (9). Now, it is widely validated that 1P and 2P absorption can be substantially different, especially in small molecules with high degree of molecular symmetry (56). The influence of parity is apparent in the absorption spectrum of azobenzene, where the centrosymmetric *trans* isomer has a dipolar electronic transition between the symmetric highest occupied molecular orbital (HOMO) and the anti-symmetric lowest unoccupied molecular orbital (LUMO). PTLs appear to retain the azobenzene electronic symmetry for a variety of ligand substituents, as seen experimentally by the similarity of 1P absorption of first generation PTLs (2). Two-photon absorption in these simple molecules can be approximated as the product of two dipolar transitions, requiring that the electronic wavefunctions in the initial and final states have the same symmetry. The reversal of parity selection rules leads to the prediction that the 1P-allowed π-π^* transition should become 2P forbidden. This prediction appears upheld by both of the first generation PTLs, as seen by their blue-shifted 2P absorption bands (Fig. 1 and *SI Appendix*, Fig. S3). Furthermore, the observation that the bent *cis* isomer of L-MAG0 had common 1P and 2P transitions is consistent with the parity formalism applied to non-centrosymmetric molecules.

It is interesting to note that the asymmetrically substituted L-MAG0$_{460}$ also showed blue-shifted 2P absorption consistent with a 2P-forbidden transition at 460 nm. Although the reduced symmetry of this photoswitch could relax the parity selection rules for π-π^* transitions, our measurements are collectively more consistent with a highly blue-shifted n-π^* band. The ordering of electronic states in pseudostilbenes is still debated (38), but electronic structure calculations on related molecules Disperse Red 1 and Disperse Orange 3 show significant population of an *n*-like HOMO-1 state (38). The character of these electronic transitions is significant for at least two reasons. First, a higher photoisomerization yield is often associated with n-π^* transition because it directly accesses the reactive excited state (42). Second, it suggests that solvent stabilization of a nonplanar *trans* conformation underlies the favorable 2P absorption in push–pull PTLs. This insight may be important in designing new 2P azobenzenes with both thermal bistability and favorable σ_2. For instance, an alternative chemistry for red-shifting azobenzene absorption is to break the symmetry of the *trans* isomer by steric

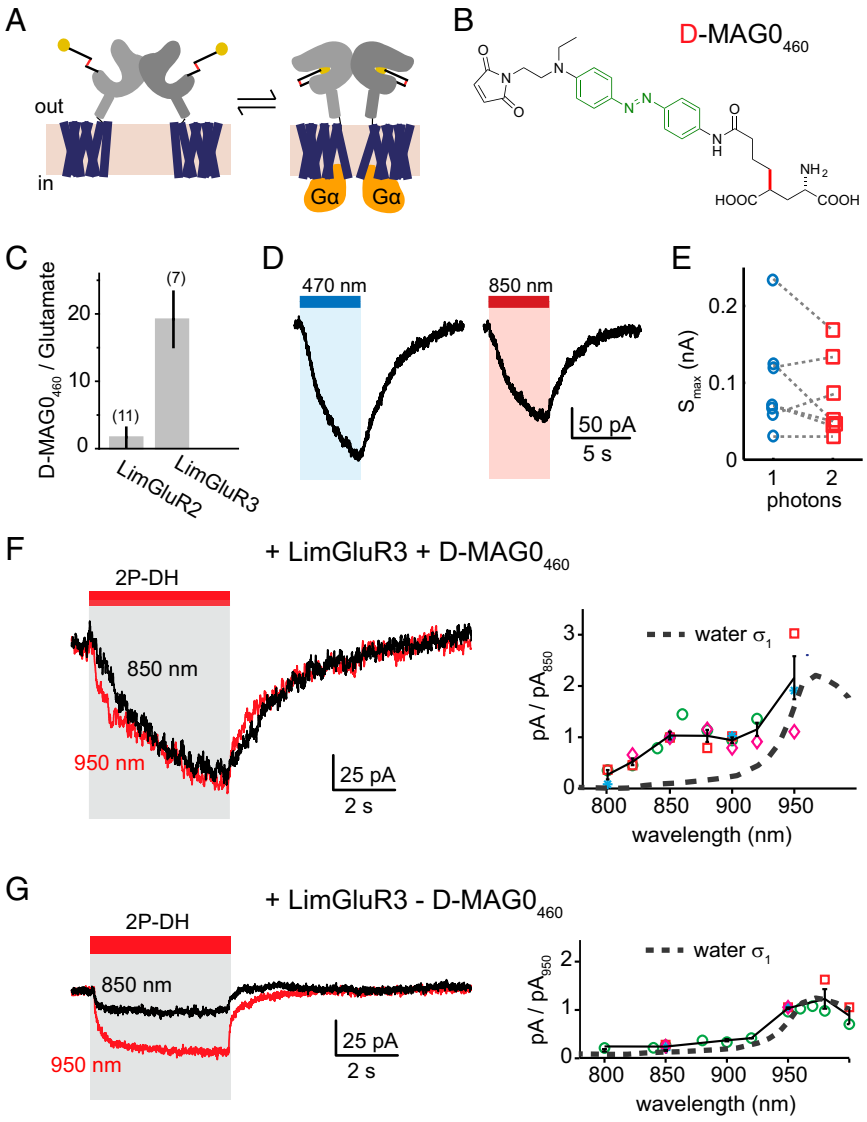

Fig. 6. Photoactivation of mGluR signaling with D-MAG0$_{460}$. (*A*) Group II metabotropic GluRs couple glutamate to a $G_{i/o}$ signaling cascade. Engineered mGluRs (LimGluRs) require MAGs with altered stereochemistry. (*B*) D-MAG0$_{460}$ is a second generation PTL with similar optical properties to L-MAG0$_{460}$. (*C*) The efficacy of D-MAG0$_{460}$ photoactivation (445 nm) in LimGluR2 and LimGluR3 was assessed as the percentage of GIRK current observed relative to saturating glutamate (1 mM). (*D*) Whole cell voltage-clamp recordings from HEK293T cells expressing LimGluR3 and labeled with D-MAG0$_{460}$ show that blue light activates a G protein signaling cascade, measurable by GIRK currents. The kinetics of the photocurrent are considerably slower than photoswitching. (*E*) Whole cell excitation by 2P-DH with 850 nm produced on average 85 ± 13% of the MAG-dependent current of wide-field 470-nm excitation ($n = 7$). (*F*) The wavelength dependence of LimGluR3 + D-MAG0$_{460}$ currents, $n > 3$ cells for all wavelengths. Each symbol represents an individual cell. Data points were first scaled by light intensity (relative to 850 nm), and then normalized to the each cell's response to 850 nm. (*G*) Additionally 2P-DH produced a relatively small inward current in some cells, independent of MAG, which had easily distinguishable kinetics and different wavelength dependence ($n > 2$ cells for all wavelengths). Each symbol represents an individual cell. Black represents mean and SEM. The action spectrum of nonspecific current increased in amplitude with longer wavelength. Accounting for the MAG-independent current, the largest MAG-dependent currents occur at a wavelength of 850 nm, functionally corroborating the measured 2P absorption spectrum of L-MAG0$_{460}$ (Fig. 1*A*).

crowding with ortho substitutions (57). It was recently demonstrated that tetra-*ortho*-chloro MAG (*to*Cl-MAG1) has both enhanced n-π* absorption in the *trans* isomer and thermal bistability in agonizing LiGluR (52). Our results suggest that such molecules may also have favorable 2P absorption. Although these ideas remain to be experimentally validated, identifying general strategies for designing 2P azobenzenes would accelerate the development of new PTLs for optical manipulation of neurophysiology. These measurements may also possibly find wider impact in industrial and research applications where azobenzenes are used as molecular photoswitches, such as optical storage (58) and optomechanical manipulation of biomolecules (59).

Summary

In summary, we have quantitatively characterized the 2P brightness of MAG PTLs with either a symmetrically or asymmetrically-substituted azobenzene core. We found that both types of MAGs have 2P absorption cross-sections that are relatively large compared with other optical tools widely used in neuroscience, and we identified functional conditions for 2P photoactivation of each MAG in conjugation with engineered ionotropic and metabotropic GluRs. We demonstrated that digital holographic 2P stimulation of MAGs can effectively be used to depolarize cells, or activate GPCR signaling cascades, with either electrophysiological or imaging readout with red-shifted genetically

encoded fluorescent indicators. These results highlight the possibility of optically mimicking elements of excitatory neurotransmission using a combination of 2P optical tools and genetically specified pharmacology that can add novel dimensions to studies of intact neural circuits.

Materials and Methods

Femtosecond Absorption Spectroscopy. Femtosecond transient absorption spectra were recorded using a home-built nonlinear spectrophotometer (*SI Appendix*, Fig. S2*A*) based on an amplified Ti:sapphire laser system (Newport; SpitfirePro), as described elsewhere (1). In brief, short pulsed light at 800 nm (2.1 W time-averaged power, 1-kHz repetition rate, 800 nm, 40-fs pulse FWHM) was split into independent optical paths to generate pump and probe pulses. Pump pulses resonant with the 1P absorption of *trans*-L-MAG0 and *trans*-L-MAG0$_{460}$ (λ_{pump} = 400 nm, <2.5 mW, 100 fs) were obtained from the fundamental pulse by second-harmonic generation in a BB0 crystal ($\theta = 29.2°$, 1 mm thick). For 2P excitation of L-MAG0$_{460}$, the pump pulse was the laser fundamental (16 mW). The probe pulse was a coherent white light generated by self-phase modulation of < 1 μJ 800 nm focused into a 2-mm-thick CaF_2 window. Pump-induced changes in absorption (ΔA) spectra were recorded for a time series of pump-probe delays with 10-fs resolution by controlling the optical path length of one pulse with a computer-controlled translation stage. At each time point, ΔA(λ, t-τ) was calculated from pairs of probe transmission spectra obtained at 1 kHz while optically chopping pump exposure at 500 Hz. Self-referenced probe transmission allowed detection changes in optical density $<10^{-4}$. Pump and probe pulses were linearly polarized at magic angle (54.8°) to obtain isotropic response. MAGs in DMSO were measured in 1-mm path at 0.5–1 OD. Photostationary states of MAGs were maintained during the pump-probe measurement by irradiating the sample cuvette with an ancillary continuous-wave laser (470 nm, <5 mW/mm^2 for L-MAG0; 530 nm, <5 mW/mm^2 for L-MAG0$_{460}$). Photoproduct accumulation between pump pulses (2 ms) was negligible. Global analysis was done with custom software written by Dr. Mikas Vengris (Vilnius University).

Two-Photon Absorption Spectrophotometry. Two-photon absorption spectra were recorded using the same laser system used for transient absorption measurements (*SI Appendix*, Fig. S2). Coherent white light pulses were generated by focusing 800-nm laser pulses into a thin windows of sapphire, YAG, or CaF_2, depending on the spectrum required. The white light pulse was necessarily limited to very low intensity to maintain linear chirp over a broad spectrum; e.g., typically <1 μJ of 800 nm fundamental pulse focused loosely into a 2-mm-thick crystalline window and passed through 2 OD Scott glass to filter out excess 800 nm yielding a white light pulse energy of <40 nJ at the sample. Short-pulsed light (70–150-fs transform-limited pulse duration) at NIR wavelengths (λ_{NIR}) were generated from an optical parametric amplifier. Wavelengths longer than 800 nm were determined by frequency-doubling pulses in BBO. The NIR pulse energy typically needed to be in the range 10–100 μJ to get reasonable signal to noise. Consequently, cross-phase modulation was considerable. We took care in the experiments to check that the time integral for the empty cuvette produced a flat background. Measurements were made in a custom cuvette made from 150-μm coverslips to hold 20–50 μL sample volume with a nominal path length of 0.7 mm. For measurement of *cis*-L-MAG0, a photostationary state with > 90% *cis* isomers was maintained by an ancillary continuous-wave laser (400 nm, <5 mW/mm^2). Laser parameters for 2P absorption measurements are summarized in *SI Appendix*, Table S1. Cross-sections were determined relative to reference samples, coumarin 153 and MNI-glutamate. Samples were measured at the following concentrations (in mM): L-MAG0 3.1 ± 0.2, L-MAG0$_{460}$ 21 ± 2, MNI-glutamate 45 ± 5, coumarin 153 20 ± 2. An extinction coefficient of *trans*-L-MAG0$_{460}$ was determined by plotting optical density vs. concentration for serial dilution of a 100-mM stock made from 2.0 mg L-MAG0$_{460}$ dissolved in anhydrous DMSO (Sigma).

Two-Photon Excitation Conditions. The 2P digital holography was done with a commercial spatial light modulator system (Phasor; Intelligent Imaging Innovations, Inc.). Holograms were calculated from user-defined ROIs based on images obtained from fluorescence images of the preparation. NIR laser pulses encoding phase holograms were projected onto the back aperture of a 20x/1.0NA water dipping objective. All optical powers were measured after the objective with a λ-calibrated piezoelectric meter (Thorlabs). Radiant flux (photon · s^{-1}) was calculated from measured power P for center wavelength λ, as:

$$I_{av} = g\frac{P}{hc/\lambda}(area)^{-1}.$$

The factor g accounted for the time distribution of photons for different light sources: LED, g = 1; 2P-DH: $g^2 = [g_p/(f\tau)]$, where we used value g_p for Gaussian pulse shape (6), repetition rate $f = 80$ MHz, and a pulse duration $\tau \sim 400$ fs, measured by autocorrelation of NIR pulses at the objective (Intelligent Imaging Innovations, Inc.). The ROI areas used to calculate light intensity for 2P-DH were determined from spatial calibration of the image within Slidebook 5.5 imaging software. Time-averaged powers at the objective for 2P-DH experiments ranged from 75 to 300 mW. Scanning excitation used NIR time-averaged power less than 20 mW (80 MHz, ca. 300 fs).

Functional Imaging. R-GECO was imaged on an upright spinning disk confocal microscope (Intelligent Imaging Innovations, Inc.) with a 561-nm diode laser and 20x/1.0NA water dipping objective (Zeiss). Images were obtained by an EM-CCD camera at frame rates of 10–20 Hz. The 2P-DH light path was coupled to the microscope through a sideport and projected onto the sample through the imaging objective. The 2P bouts were controlled by a Pockel's cell and timed with camera acquisition through Slidebook imaging software. Ca^{2+} transients represent mean ΔF/F over pixels within ROIs.

Data Analysis. All spectroscopy and physiology data analysis was done with custom scripts in Matlab. All values represent mean ± SEM. Errors on calculated values were determined using SE propagation, unless otherwise stated.

Details of tissue culture, electrophysiology, and MAG synthesis are provided in *SI Appendix*.

ACKNOWLEDGMENTS. We thank Matthew Banghart for the generous gift of MAQ; Olivier Thoumine, Cherise Stanley, and Grant Kauwe for the low-affinity GluK2 construct (LA-LiGluR); Andreas Reiner for guidance on working with D-MAG0$_{460}$; Hillel Adesnik for electrophysiology data acquisition software; and Karl Kilborn and Brian Bodenmeister for customizing Slidebook software. Funding was provided by the NIH Nanomedicine Development Center for the Optical Control of Biological Function (PN2EY018241) (to E.Y.I.), NIH Ruth L. Kirschstein National Research Service Award (F32EY022840) (to M.A.K.), and the National Science Foundation (CHE-1413739) (to D.S.L.).

1. Miesenböck G (2011) Optogenetic control of cells and circuits. *Annu Rev Cell Dev Biol* 27(1):731–758.
2. Kramer RH, Mourot A, Adesnik H (2013) Optogenetic pharmacology for control of native neuronal signaling proteins. *Nat Neurosci* 16(7):816–823.
3. Oheim M, Beaurepaire E, Chaigneau E, Mertz J, Charpak S (2001) Two-photon microscopy in brain tissue: Parameters influencing the imaging depth. *J Neurosci Methods* 111(1):29–37.
4. Helmchen F, Denk W (2005) Deep tissue two-photon microscopy. *Nat Methods* 2(12): 932–940.
5. Denk W, Strickler JH, Webb WW (1990) Two-photon laser scanning fluorescence microscopy. *Science* 248(4951):73–76.
6. Helmchen F, Fee MS, Tank DW, Denk W (2001) A miniature head-mounted two-photon microscope. High-resolution brain imaging in freely moving animals. *Neuron* 31(6):903–912.
7. Svoboda K, Yasuda R (2006) Principles of two-photon excitation microscopy and its applications to neuroscience. *Neuron* 50(6):823–839.
8. Mank M, et al. (2008) A genetically encoded calcium indicator for chronic in vivo two-photon imaging. *Nat Methods* 5(9):805–811.
9. Lakowicz JR (1997) *Topics in Fluorescence Spectroscopy: Nonlinear and Two-Photon-Induced Fluorescence* (Plenum Press, New York).
10. Andrasfalvy BK, Zemelman BV, Tang J, Vaziri A (2010) Two-photon single-cell optogenetic control of neuronal activity by sculpted light. *Proc Natl Acad Sci USA* 107(26): 11981–11986.
11. Prakash R, et al. (2012) Two-photon optogenetic toolbox for fast inhibition, excitation and bistable modulation. *Nat Methods* 9(12):1171–1179.
12. Rickgauer JP, Tank DW (2009) Two-photon excitation of channelrhodopsin-2 at saturation. *Proc Natl Acad Sci USA* 106(35):15025–15030.
13. Oron D, Papagiakoumou E, Anselmi F, Emiliani V (2012) Two-photon optogenetics. *Prog Brain Res* 196:119–143.
14. Ellis-Davies GCR (2011) Two-photon microscopy for chemical neuroscience. *ACS Chem Neurosci* 2(4):185–197.
15. Xu C, Guild J, Webb W, Denk W (1995) Determination of absolute two-photon excitation cross sections by in situ second-order autocorrelation. *Opt Lett* 20(23): 2372–2374.
16. Xu C, Webb WW (1996) Measurement of two-photon excitation cross sections of molecular fluorophores with data from 690 to 1050 nm. *J Opt Soc Am B* 13(3): 481–491.

17. Drobizhev M, Makarov NS, Tillo SE, Hughes TE, Rebane A (2011) Two-photon absorption properties of fluorescent proteins. *Nat Methods* 8(5):393–399.
18. Shaner NC, Steinbach PA, Tsien RY (2005) A guide to choosing fluorescent proteins. *Nat Methods* 2(12):905–909.
19. Bartels E, Wassermann NH, Erlanger BF (1971) Photochromic activators of the acetylcholine receptor. *Proc Natl Acad Sci USA* 68(8):1820–1823.
20. Lester HA, Chang HW (1977) Response of acetylcholine receptors to rapid photochemically produced increases in agonist concentration. *Nature* 266(5600):373–374.
21. Volgraf M, et al. (2006) Allosteric control of an ionotropic glutamate receptor with an optical switch. *Nat Chem Biol* 2(1):47–52.
22. Gorostiza P, et al. (2007) Mechanisms of photoswitch conjugation and light activation of an ionotropic glutamate receptor. *Proc Natl Acad Sci USA* 104(26):10865–10870.
23. Szobota S, et al. (2007) Remote control of neuronal activity with a light-gated glutamate receptor. *Neuron* 54(4):535–545.
24. Caporale N, et al. (2011) LiGluR restores visual responses in rodent models of inherited blindness. *Mol Ther* 19(7):1212–1219.
25. Numano R, et al. (2009) Nanosculpting reversed wavelength sensitivity into a photoswitchable iGluR. *Proc Natl Acad Sci USA* 106(16):6814–6819.
26. Li D, Hérault K, Isacoff EY, Oheim M, Ropert N (2012) Optogenetic activation of LiGluR-expressing astrocytes evokes anion channel-mediated glutamate release. *J Physiol* 590(Pt 4):855–873.
27. Sandoz G, Levitz J, Kramer RH, Isacoff EY (2012) Optical control of endogenous proteins with a photoswitchable conditional subunit reveals a role for TREK1 in GABA(B) signaling. *Neuron* 74(6):1005–1014.
28. Izquierdo-Serra M, Trauner D, Llobet A, Gorostiza P (2013) Optical modulation of neurotransmission using calcium photocurrents through the ion channel LiGluR. *Front Mol Neurosci* 6:3.
29. Kauwe G, Isacoff EY (2013) Rapid feedback regulation of synaptic efficacy during high-frequency activity at the Drosophila larval neuromuscular junction. *Proc Natl Acad Sci USA* 110(22):9142–9147.
30. Levitz J, et al. (2013) Optical control of metabotropic glutamate receptors. *Nat Neurosci* 16(4):507–516.
31. Kienzler MA, et al. (2013) A red-shifted, fast-relaxing azobenzene photoswitch for visible light control of an ionotropic glutamate receptor. *J Am Chem Soc* 135(47): 17683–17686.
32. Izquierdo-Serra M, et al. (2014) . Two-photon neuronal and astrocytic stimulation of azobenzene-based photoswitches. *J Am Chem Soc* 136(24):8693-8701.
33. Mourot A, et al. (2011) Tuning photochromic ion channel blockers. *ACS Chem Neurosci* 2(9):536–543.
34. Bègue A, et al. (2013) Two-photon excitation in scattering media by spatiotemporally shaped beams and their application in optogenetic stimulation. *Biomed Opt Express* 4(12):2869–2879.
35. Zhao Y, et al. (2011) An expanded palette of genetically encoded Ca^{2+} indicators. *Science* 333(6051):1888–1891.
36. De Boni L, Misoguti L, Zilio SC, Mendonça CR (2005) Degenerate two-photon absorption spectra in azoaromatic compounds. *ChemPhysChem* 6(6):1121–1125.
37. Rau H (1973) Spectroscopic properties of organic azo compounds. *Angew Chem Int Ed Engl* 12(3):224–235.
38. Silva DL, Krawczyk P, Bartkowiak W, Mendonça CR (2009) Theoretical study of one- and two-photon absorption spectra of azoaromatic compounds. *J Chem Phys* 131(24): 244516.
39. Yamaguchi S, Tahara T (2003) Two-photon absorption spectrum of all-trans retinal. *Chem Phys Lett* 376(1–2):237–243.
40. Trigo FF, Corrie JET, Ogden D (2009) Laser photolysis of caged compounds at 405 nm: Photochemical advantages, localisation, phototoxicity and methods for calibration. *J Neurosci Methods* 180(1):9–21.
41. van Stokkum IHM, Larsen DS, van Grondelle R (2004) Global and target analysis of time-resolved spectra. *Biochim Biophys Acta* 1657(2-3):82–104.
42. Bandara HMD, Burdette SC (2012) Photoisomerization in different classes of azobenzene. *Chem Soc Rev* 41(5):1809–1825.
43. Fujino T, Arzhantsev SY, Tahara T (2001) Femtosecond time-resolved fluorescence study of photoisomerization of trans-azobenzene. *J Phys Chem A* 105(35):8123–8129.
44. Weston MC, Gertler C, Mayer ML, Rosenmund C (2006) Interdomain interactions in AMPA and kainate receptors regulate affinity for glutamate. *J Neurosci* 26(29): 7650–7658.
45. Reiner A, Isacoff EY (2014) Tethered ligands reveal glutamate receptor desensitization depends on subunit occupancy. *Nat Chem Biol* 10(4):273–280.
46. Fortin DL, et al. (2008) Photochemical control of endogenous ion channels and cellular excitability. *Nat Methods* 5(4):331–338.
47. Dascal N (1997) Signalling via the G protein-activated K+ channels. *Cell Signal* 9(8): 551–573.
48. Palmer KF, Williams D (1974) Optical properties of water in the near infrared. *J Opt Soc Am* 64(8):1107–1110.
49. Shapiro MG, Homma K, Villarreal S, Richter C-P, Bezanilla F (2012) Infrared light excites cells by changing their electrical capacitance. *Nat Commun* 3:736.
50. Callaway EM, Yuste R (2002) Stimulating neurons with light. *Curr Opin Neurobiol* 12(5):587–592.
51. Yao J, Liu B, Qin F (2009) Rapid temperature jump by infrared diode laser irradiation for patch-clamp studies. *Biophys J* 96(9):3611–3619.
52. Mattis J, et al. (2012) Principles for applying optogenetic tools derived from direct comparative analysis of microbial opsins. *Nat Methods* 9(2):159–172.
53. Lin JY, Knutsen PM, Muller A, Kleinfeld D, Tsien RY (2013) ReaChR: A red-shifted variant of channelrhodopsin enables deep transcranial optogenetic excitation. *Nat Neurosci* 16(10):1499–1508.
54. Papagiakoumou E, et al. (2010) Scanless two-photon excitation of channelrhodopsin-2. *Nat Methods* 7(10):848–854.
55. Olson JP, Banghart MR, Sabatini BL, Ellis-Davies GCR (2013) Spectral evolution of a photochemical protecting group for orthogonal two-color uncaging with visible light. *J Am Chem Soc* 135(42):15948–15954.
56. Birge RR (1986) Two-photon spectroscopy of protein-bound chromophores. *Acc Chem Res* 19(5):138–146.
57. Beharry AA, Sadovski O, Woolley GA (2011) Azobenzene photoswitching without ultraviolet light. *J Am Chem Soc* 133(49):19684–19687.
58. García-Amorós J, Velasco D (2012) Recent advances towards azobenzene-based light-driven real-time information-transmitting materials. *Beilstein J Org Chem* 8: 1003–1017.
59. Beharry AA, Woolley GA (2011) Azobenzene photoswitches for biomolecules. *Chem Soc Rev* 40(8):4422–4437.
60. Rullo A, et al. (2014) Long wavelength optical control of glutamate receptor ion channels using a tetra-ortho-substituted azobenzene derivative. *Chem Commun (Camb)* 50(93):14613–14615.